International Journal of
INTELLIGENT SYSTEMS AND APPLICATIONS IN ENGINEERING
ISSN:2147-6799 www.ijisae.org Original Research Paper

Tuberculosis Detection using X-Ray Images based on DbneAlexNet with Tangent Chef Leader Optimization

Roopa N. K.*[1], Mamatha G. S.[2]

Submitted:12/03/2024 **Revised**: 27/04/2024 **Accepted**: 04/05/2024

Abstract: Tuberculosis (TB) is a part of lung infection, which arises by the bacterial infectivity and it causes the major death in the globe. The precise and early detection of TB is necessary, if not, it may perhaps too severe. Presently, the TB detection process by chest X-ray (CXR) images has some difficulties to set up in low-cost embedded devices and personal computer. To overcome this issue, the optimization enabled DbneAlexNet based TB detection is proposed in this research. At the beginning stage, the input CXR image is applied to image pre-processing, in which the adaptive wiener filter (AWF) is hired to diminish the noise. Here, the Double-Net is adopted for the segmentation of TB affected region from the CXR image. Moreover, the parameters of Double-Net are trained by the proposed Chef Leader Based Optimization (CLBO). Furthermore, feature extraction process is accomplished for extracting the relevant features. At last, the TB disorder is detected by the DbneAlexnet, where the proposed Tangent Chef Leader Based Optimization (TCLBO) is designed for the training of DbneAlexnet. Furthermore, the TB detection is evaluated in connection with the metrics such as accuracy, Positive Predictive Value (PPV), Negative Predictive Value (NPV), True Positive Rate (TPR) and True Negative Rate (TNR) with the superior values like 0.991, 0.964, 0.958 0.993, and 0.968 are observed.

Keywords: *Chest X-ray images, Chef Based Optimization, DbneAlexNet, Double-Net, Hybrid Leader-Based Optimization*

1. Introduction

TB is a severe infective disorder which primarily infects the lungs. The majority of the indication can be predicted by appraising the CXR images of TB affected persons. TB has some visual signs like fibrosis, consolidation, infiltration, mass, nodule, pneumonia and pleural thickening, etc., [1]. Moreover, TB is the fifth major reason for death, which is an infectious illness that affects the entire population and it is a chronic and spreadable illness. It is typically originated by the Mycobacterium tuberculosis bacteria and it mostly infects the human lungs. TB can spread in the atmosphere through everybody due to the sneezing, coughing, and spitting of TB patients spreads throughout the air. Each year, approximately one-third part of world's population is infected by Mycobacterium tuberculosis at an average rate of one percent of total population [2]. According to the World Health Organization (WHO), about 10 million individuals were diagnosed with TB during 2018, with 1.45 million deaths [3]. It is mainly due to the spreading of coughing and sneezing of a person who has a vigorous form of TB [4]. When the tuberculosis passes through body, a time period required to cause the disease and the probability of its development differs from person to person. Particularly, the individuals with low immunity are highly susceptible by this illness [5].

TB is generally diagnosed using a variety of medical assessments including bio-images. The CXR images are commonly used to segment affected lung region. Furthermore, CXR is a critical and faster diagnostic tool for TB detection. Because of the differing form of disease, TB prediction using CXR is a difficult task that necessitates the aid of experts. TB disorder was predicted by applying CAD and CXR. It can minimize the mortality rates, particularly in resource-limited areas [1]. TB lost the lives of 1.4 million people worldwide, and this report revealed that ten million of people were identified as TB positive cases. The majority of those affected with tuberculosis (>90%) are adults, with males are infected more than females. Additionally, this report confirms that approximately 25% of the world's population encompasses with TB. In most cases, TB is treatable and preventable when discovered in its early stages, and >85% of people who contract TB are able to recover completely [1]. The severity of TB is then determined from the recorded image using a computer algorithm or a medical professional [6] [4]. Chest radiographs are regularly done in hospitals as one of the important medical imaging techniques for diagnosing the problems in chest. Furthermore, the segmentation of lung region from the CXR is a crucial part of CAD process. The effective lung segmentation method is shape-model or atlas-based image segmentation [7].

The early detection and appropriate treatment may preserve the human life and increase the duration of life. Nonetheless, the lack of clinical tools in the the developing

[1] *Visvesvaraya Technological University, Belagavi 590018, India*
ORCID ID : 0009-0007-8169-4794
[2] *Visvesvaraya Technological University, Belagavi 590018, India*
ORCID ID : 0000-0003-2679-784X
* *Corresponding Author Email: roopank@ssit.edu.in*

world made the detection as a difficult task. As a result, accurate identification of tuberculosis is essential for preventing its propagation [6] [4]. The tuberculin skin test (TST), Microscopy, culture test, interferon-g release assay (IGRA) and GeneXpert the well-established TB detection methods [8]. Furthermore, a lot Deep Learning (DL) as well as Machine Learning (ML) methods have been established and applied for estimating the CXR image. When compared to ML, the DL-assisted model is employed for achieving higher detection accuracy [4] [8]. Convolutional Neural Networks (CNNs) is a sophisticated DL architecture that has the ability of detecting the pulmonary tuberculosis from CXR images. CNNs have demonstrated their abilities in image classification and have been successfully employed in illness diagnosis, such as the detection of pleural effusion and cardiomegaly on chest radiography [9]. In addition to the DL technique, ensemble learning combines the outcomes of multiple learning models to improve the prediction of TB disorder [10]. Moreover, the DL approach in conjunction with genetic algorithms, artificial immune system and fuzzy logic has more efficiency of TB diagnosis. In addition, the DL method was used to construct a mobile health solution to improve the TB diagnosis in underserved and underdeveloped countries [11]

The main aim of this research is to attain a reliable method for TB detection utilizing CXR images known as TCLBO_DbneAlexNet. Here, the AWF is used in the preprocessing stage, so that the undesirable noise from the image is eliminated. After that, Double U Net is hired to segment the images and the CLBO is utilized for the train phase of Double U Net classifier. Following this, the Grey Level Co-occurrence Matrix (GLCM),the geometric features like area, perimeter, and irregularity index; Discrete Wavelet Transform (DWT), Compound Local Binary Pattern (CLBP), Pyramid Histogram of Orientation (PHoG) features, Local Vector Pattern (LVP),Local Optimal Oriented Pattern (LOOP), Local directional ternary pattern (LDTP) features are extracted. At last, the TB detection is CXR images are stated in section 2 and the proposed model for TB detection is described in section 3. Moreover, section 4 covers the experimental done by the DbneAlexNet and its parameters are fine-tuned using the developed TCLBO. Furthermore, the predictive analysis is executed from the TB detected outcome to classify the TB class, heat maps for localization, and to determine the lung abnormalities.

The major contribution of this research is explicated as follows

- **Proposed CLBO_Double U Net for affected lung region segmentation**: The lung region is segmented with the help of Double U Net, in which its parameters are tuned using the CLBO algorithm. Here, the CLBO is designed by the integration process of chef based optimization (CLBO) and hybrid leader optimization (HLBO).
- **Proposed TCLBO_DbneAlexNet for TB detection:** A novel model developed for TB detection is based on hybrid optimization enabled DL model termed as TCLBO_DbneAlexNet. Here, the parameter of DbneAlexNet is optimized using the TCLBO. The merging of Tangent Search Algorithm (TSA) and CLBO forms the proposed TCLBO. The outstanding section of this paper is stated as follows: The motivation and existing approaches associated with TB detection using outcomes and assessment of existing and proposed method. The conclusion part is explicated in section 5.

2. Motivation

The time delayed identification of tuberculosis raises their chance of infecting others. If it is diagnosed at the curable stage, then appropriate treatment is provided. Hence the patient has a seventy to eighty percent of probability to cure this disease. Several methods were employed for the earlier prediction of TB. Still, they are expensive and take more time for computation. Therefore, the hybrid optimization-based DL approach is utilized for TB detection.

2.1. Literature survey

An,L. *et al*. [3] developed a lightweight tuberculosis recognition model (E-TBNet) for the detection of TB disorder. At the beginning stage, the image distribution process of the TB repositories was evaluated, and then the basic residual module was augmented in the second stage. Finally, an efficient attention mechanism was developed for merging the channel features. This method was simple to implement the devices with limited hardware. However, this approach did not succeed for exploring enormous number of datasets. Khatibi T.*et al*. [12] developed a unique approach for TB classification from chest radiographs (CXR) images based on CNN termed as complex networks, and stacked ensemble (CCNSE). Here, the image was classified into abnormal and normal form of TB using a stacked ensemble network. For detecting the questionable locations, it did not require the segmentation technique. Furthermore, it was used as a Computer Aided Design (CAD) model for minimizing effort on medical experts and the processing time. In addition, CCNSE was more helpful for diminishing the computational time and the error occurred in image categorization. Still, it did not access the scalability of this technique to large databases. Kadry, S. *et al*. [1] devised a VGG-UNet-supported segmentation and classification strategy for TB detection. The Spotted Hyena Algorithm (SHA) was used to determine the best attributes. This model improved the accuracy while requiring relatively a minimum training time. Still, this method was failed to validate in multiple

CXR datasets. Ayaz, M. *et al*. [4] developed the ensemble learning based TB detection. Here, the deep features were merged with hand-crafted features (HF) to form the ensemble classifiers. Moreover, the hand-crafted features were sophisticated by a Gabor filter, while a pre-trained CNNs were used to refine the features. Hence, this model was employed as a useful screening material for diagnosing the TB disorder. However, this approach was failed to consider a specific hand-crafted feature for creating a superior feature set to improve the detection process. Urooj, S.,*et al*. [5] devised Stochastic Learning based Artificial Neural Network (SL-ANN) model for TB detection. This method was employed for learning the features of CXR images and ANN parameters. Moreover, the model weights were initialized by a random beginning point. In this method, the error rate was low. Still, it was failed for rapid identification and distinguishing the proportion of disease evolution. Rahman, M., *et al*. [29] developed the TB detection using Deep pre-trained networks developed the hybrid approach-based TB detection. Here, the CXR images were given to the image preprocessing technique. Moreover, the pre-trained networks like VGG19, DenseNet201 and ResNet101, were employed for extracting the features of CXR images. Furthermore, the eXtreme Gradient Boosting (XGBoost) model was adopted for classifying the TB and regular cases. Ravi, V., *et al*. [9] devised the multi-channel EfficientNet for TB detection. Here, the features of EfficientNet models were incorporated. Afterwards, the fused features were sent through many non-linear fully linked layers, and then, these features were fed to the stacked ensemble learning classifier to detect the TB disease. However, some mis-classification occurred in TB detection process. Fati, S.M., *et al*. [15] developed the hybrid learning approach-based TB detection. Here, two techniques were developed, in which the first technique utilized a hybrid approach using the GoogLeNet CNN, ResNet-50 and support vector machine (SVM) algorithm. In the second approach, the artificial neural network (ANN) was employed, in which the GLCM, DWT LBP features were extracted to yield the superior result. However, it was failed due to limited images of dataset.

2.2. Major challenges

The challenges of existing TB detection methods using CXR images are described as follows,

- The design [13] of light weight structure for diminishing the hardware stage was considered as the major challenge in E-TBNet. Additionally, the narrow networking of E-TBNet affects the training process.
- The CCNSE model [12] was developed for the analysis of large networks and it has high time complexity and required more memory. Furthermore, this approach was utilized to increases the TB diagnosis rate. Additionally, this method failed to use the global complex structure for ensuring minimum time complexity.
- The VGG-UNet model [1] demonstrated a binary classification using a fine-tuned classifier for achieving high accuracy. However, this approach estimated the artefact-ignored image as the adequate HF.
- The ensemble learning [4] using CXR images were developed to identify the TB. Although the performance of a single CNN feature extractor was uneven, it was higher for huge datasets.

3. proposed tclbo_dbnealexnet for tb detection

The main attention of this work is to perform the TB detection process using optimized DbneAlexNet. Initially, input CXR image is collected from a database is applied to pre-processing step. In the preprocessing phase, an adaptive wiener filter [12] is used to remove unwanted error and noise. Afterwards, the noise free image is forwarded to the image segmentation stage, where Double-Net is utilized to segment the lung part in the CXR image. Here, the Double-Net [13] is trained by the CLBO. Afterward, feature extraction is performed for reducing the number of resources required to describe a large set of images, wherein the features such as GLCM features [14] like entropy, contrast, correlation, Angular Second Moment (ASM) and energy; CLBP [15], DWT [16], LVP [17], PHoG [18]LOOP[19], LDTP [20], and geometric features [21], like area, perimeter, and irregularity index are extracted. Finally, TB is detected based on DbneAlexnet [22], where the DbneAlexnet is trained by the proposed TCLBO. Figure 1 reveals the block diagram of proposed TCLBO_DbneAlexnet for TB detection.

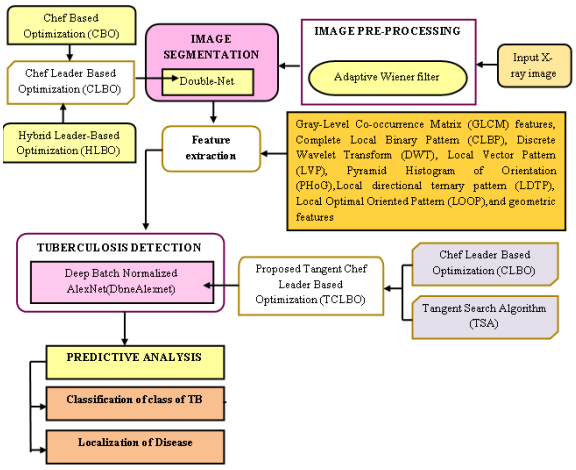

Fig. 1. Block diagram of the proposed TCLBO_DbneAlexnet for TB detection by CXR images.

3.1. Image Acquisition

The CXR image is collected from the dataset Q, where the entire counting of images presented in the dataset is denoted as V. Here, the dataset is defined as,

$$Q=\left\{Q_1,Q_2,...,Q_p,...,Q_v\right\} \quad (1)$$

Here, v implies the overall images and the p^{th} image Q_p are employed for the TB detection process.

3.2. Image pre-processing by Adaptive Wiener Filter

For diminishing the noisy part of an image, the image preprocessing technique is utilized. Usually, the images collected from the dataset have some default noise. Hence, it must be neglected to obtain the noiseless image. Here, the AWF [12] is adopted to do this noise removal process. Moreover, AWF is a widespread image denoising technique, which utilized a statistical and central pixel. It provided a restored image with superior quality and modifies the output in connection with a local variance of image. Here, the mean square error (MSE) amongst the original and the restored images are minimized and it is used to maintain the high-frequency as well as edge regions of the image.

3.1.1. Adaptive Wiener filter

The noise from the image is eliminated by AWF [12] according to the local fluctuation of images. The input CXR image Q_p is fed to the AWF. The fundamental procedure of filtering is the fall of MSE between the original and restored images. Furthermore, it is needed for conserving the edge region and frequency level of the image. Let us assume that, the images are affected by a signal-to-noise. This problem can be represented by an intendent noise, which is denoted as,

$$a\left(x,z\right)=i\left(x,z\right)+jx\left(x,z\right) \quad (2)$$

Where, the noisy measure is specified as $a\left(x,z\right)$, the noiseless image is represented as $i\left(x,z\right)$, and $j\left(x,z\right)$ signifies the additive noise. Here, the main focus of the filter is to eliminate the noise $a\left(x,z\right)$. In every image, both the variance and mean of a pixel is determined via several window sizes, in which the window exhibiting the smallest mean is selected as the optimal class. Furthermore, the filter template was selected adaptively as per the section. Here, the small and large window filters are employed in detail and smooth parts. Furthermore, it was employed to increase the filtering efficiency where as it keeps the edge and texture parts. The output results of the filtering are represented by the following equation.

$$\eta\left(x,z\right)=\Psi+\left(1-\vartheta+\Upsilon\right)*\left(\alpha\left(x,z\right)-\Psi\right) \quad (3)$$

$$\vartheta=\frac{\chi_{avr}}{\chi_{\text{var}}+1} \quad (4)$$

$$\Upsilon=\frac{\chi_{avr}}{\chi_{var}+\chi_{\max}+1} \quad (5)$$

Where, $\eta\left(x,z\right)$ represents an output pixel, $\alpha\left(x,z\right)$ specifies an original pixel, χ_{avr} indicates a mean value of a selected window, χ_{var} showed the current pixel variance. Here, $\chi_{\max}$ displays the higher variance of each pixel. For experiment, the parameter Ψ is set as 0. Moreover, the filtered output image is specified as Q_w.

3.3. Image Segmentation using Double U-Net

The filtered image Q_w is fed as an input of segmentation, in which the Double U-Net [13] is utilized to isolate infected part. In segmentation stage, the affected lungs having some injuries present in the parenchyma, which affects the respiratory. Hence, the segmentation is employed to predict the infected regions with the aid of Double U-Net model.

3.3.1. Architecture of Double U-Net

Figure 2 deliberated the double U-Net [13] architecture for segmenting the injured lung region using a chest radiograph, where, the boundary information and lung regions are combined. Moreover, the double U-Net comprises two dissimilar U-Net that is layered with each other for generating a superior outcome while compared to a single U-Net architecture. Moreover, the double U- Net comprising a 3×3 convolutional layers, which are followed by the batch normalization layer and Max Pooling, layers. Here, the 3×3 convolutions are carried out with a stride of 1. In this process, each path has five stages and five feature resolutions. The filtered image Q_w of the lung region is forwarded to the first section of the architecture, where the essential operations are performed. Afterwards, this image is incorporated with an input image, and then it is forwarded to the next section of the architecture. At the end stage of this process, the segmented image Q_s^{DUN} is gathered.

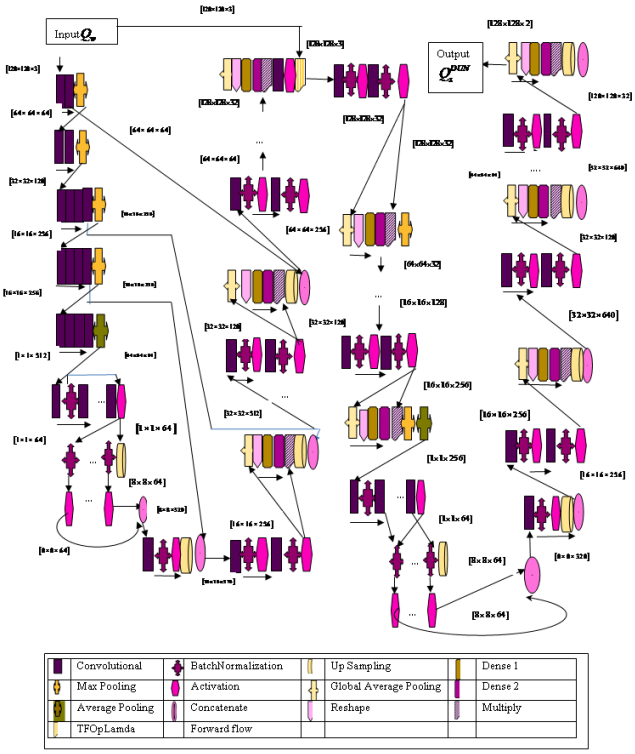

Fig. 2. Architecture of Double U-Net

3.3.2. Training of Double U-Net using CLBO

To achieve a precise segmentation, the Double U-Net classifier is trained using the developed CLBO, which is created by combining the features of CBOA [23] and HLBO [24]. CBOA is based on the development of cooking skills provided by the training classes. This method was employed for enhancing the capacity of local and global search during the exploitation and exploration phases. Moreover, the HLBO is incorporated to CBOA to attain the rapid convergence. Furthermore, the HLB involves the supervision of hybrid leader. Here, the hybrid leader is used to guide and update every member. The hybrid leader is created by a random member, best member, and a corresponding member. Here, the population members have the capability to enhance their location to attain better solutions. Hence, the integration of CBOA and HLBO effectively resolve the optimization issues and providing a balance among the exploration and exploitation phases.

Step 1: Population initialization

The individuals who like to do cooking are going attend the cooking institutes for learning different cooking methods. They can improve their ability and becoming as the chef. The goal is to select the superior candidate solution by a continuous procedure in which a large number of candidate solutions are formulated. As a result, the basic concept of CBOA is the technique of transforming a cooking student as best chef. Here, various chef teachers are present in the school, where the instructors teach the students to improve their cooking skills. Moreover, the CBO primarily consists of two types of people such as chef instructors and the cookery students. Here, CBOA member indicates a vector, whereas a set of CBOA candidates are defined below.

$$T=\begin{bmatrix} T_1 \\ \vdots \\ T_m \\ \vdots \\ T_G \end{bmatrix}_{G\times q}=\begin{bmatrix} t_{1,1} & \cdots & t_{1,n} & \cdots & t_{1,q} \\ \vdots & \ddots & \vdots & \iddots & \vdots \\ t_{m,1} & \cdots & t_{m,n} & \cdots & t_{m,q} \\ \vdots & \iddots & \vdots & \ddots & \vdots \\ t_{G,1} & \cdots & t_{G,n} & \cdots & t_{G,q} \end{bmatrix}_{G\times q} \tag{6}$$

Here, the population matrix of CBOA is specified as T, $T_m=\left(t_{m,1},t_{m,2},...,t_{m,q}\right)$ describes the m^h member, $t_{m,n}$ specifies the m^{th} solution of n^{th} coordinate. Moreover, G and q indicates the population dimension as well as the quantity of problem variables. Here, the position of CBOA members is initialized as $m=1,2,...,G$ and $n=1,2,..,q$ by the following equation,

$$t_{m,n}=B_n^{\ell}+\rho.\left(B_n^{\upsilon}-B_n^{\ell}\right) \tag{7}$$

Where, ρ indicates an un-uniform number in (0, 1) range. Moreover, B_n^{υ} and B_n^{ℓ} represents the upper and lower bounds of n^{th} variable.

Step 2: Estimation of objective factor

The fitness function is used to predict the best solution, and the updated process depends upon the objective function, which is demarcated as the distinction among the desired and the segmented output obtained using Double U Net.

$$Fitness\ \delta=\frac{1}{v}\sum_{s=1}^{v}\left[Q_s^*-Q_s^{DUN}\right]^2 \tag{8}$$

Where, v indicates the entire CXR samples covered by the dataset, Q_s^* denotes the targeted outcome and the Double U Net outcome is indicated as Q_s^{DUN}.

Step 3: Update the group of chef instructors

When the algorithm is preceded, the steps are progressively employed to the candidates. Because the CBOA candidates involved for cooking students and the chef instructors. Here, the update mechanism of these two groups is completely different due to the objective function. Initially, G_h is defined as the set of chef instructors, $G-G_h$ is represented the cooking students. Therefore, the population matrix of CBOA is indicated as,

$$TD=\begin{bmatrix} TD_1 \\ \vdots \\ YD_{G_h} \\ TD_{G_{h+1}} \\ \vdots \\ TD_G \end{bmatrix}_{G\times q}=\begin{bmatrix} td_{1,1} & \cdots & td_{1,n} & \cdots & td_{1,q} \\ \vdots & \ddots & \vdots & \iddots & \vdots \\ td_{G_h,1} & & td_{G_h,n} & & td_{G_h,q} \\ td_{G_{h+1},1} & \cdots & td_{G_{h+1},n} & \cdots & td_{G_{h+1},q} \\ \vdots & \iddots & \vdots & \ddots & \vdots \\ td_{G,1} & \cdots & td_{G,n} & \cdots & td_{G,q} \end{bmatrix}_{G\times q} \quad (9)$$

Here, G_h denotes the total count of chef instructors and TD implies the stored population matrix for CBOA. Here, the members from TD_1 to TD_{G_h} indicate a group of chef instructors and the set of cooking student is represented as $TD_{G_{h+1}}$ to TD_G.The Chef instructors typically utilized two ways to help the students for improving their cooking abilities. They initially emulate the abilities of top cooling instructor. The advancement chef teachers improve their efficiency based on the best chef instructor. Here, the updated location of different chef instructor is given as,

$$td_{m,n}^{h/D1}=td_{m,n}+\rho.\left(B_n-o.td_{m,n}\right) \quad (10)$$

Where, the updated status for m^{th} stored individual of CBOA depends on the early stage $(h/D1)$ to upgrade the chef instructor $TD_m^{h/D1}$, $td_{m,n}^{h/D1}$ specifies the n^{th} variable, the best chef instructor is denotes as C_{best}. Furthermore, z is a randomly selected number throughout the setup from a group $\{1,2\}$. This updated position is observed, if it boosts the fitness value, which is expressed below,

$$TD_m=\begin{cases} TD_m^{h/D1}, & \delta S_m^{h/D1}<\delta_m; \\ TD_m, & else \end{cases} \quad (11)$$

Here, $\delta D_m^{h/D1}$ specifies the objective factor of $TD_m^{h/D1}$.

Following that, each chef instructor increases their cooking knowledge through their practices and self-activities. The major advantages of this updating stage are to locate the optimum solution. As a result, the updated position is provided by,

$$td_{m,n}^{h/D2}=td_{m,n}+B_n^{\ell,local}+\rho.\left(B_n^{\upsilon,local}-B_n^{\ell,local}\right), m=1,2,...G_h,\ n=1,2,...,q \quad (12)$$

Where,

$$B_n^{\upsilon,local}=\frac{B_n^{\upsilon}}{r} \quad (13)$$

$$B_n^{\ell,local}=\frac{B_n^{\ell}}{r} \quad (14)$$

$$TD_m=\begin{cases} TD_m^{h/D2}, & \delta D_m{}^{h/D2}<\delta_m; \\ TD_m, & else, \end{cases} \quad (15)$$

Where, $TD_m^{h/D2}$ implies the predicted status for m^{th} CBOA candidate depends on the second phase $(h/D2)$, whereas the fitness is denoted as $\delta D_m^{h/D2}$. Here, the iteration count is specified as r.

Step 4: Update the set of cooking students

The cooking students utilized three stages in learning, where the HLBO is included in first stage. The individual cooking learners randomly select a class instructor during the first phase. Hence, the updated solution is specified as,

$$t_{m,n}(r+1)=\frac{1}{2\rho.o}\left[\rho.L_{m,n}^H(1-\rho.o)+\rho.I_{u_{m,n}}(1+\rho.o)\right] \quad (16)$$

Here, o indicates an integer which is randomly picked among $[1,2]$. This current position replaces of CBOA candidate's earlier position, if it enhanced the fitness,

$$TD_m=\begin{cases} TD_m^{D/D1}, & \delta D_m^{D/D1}<\delta_m; \\ TD_m, & else, \end{cases} \quad (17)$$

Here, $\delta D_m^{D/D1}$ defines the objective value of $TD_m^{D/D1}$.

The cooking student carefully detects and implements the cooking knowledge of chef instructors during the second phase. The following calculation is used to identify the updated location for each CBOA cooking student,

$$td_{m,n}^{D/D2}=\begin{cases} I_{u_{m,n}}, n=1; \\ td_{m,n}, \ else \end{cases} \quad (18)$$

If the fitness is enhanced, the location is replaced as,

$$TD_m=\begin{cases} TD_m^{D/D2}, & TD_m^{D/D2}<\delta_m; \\ TD_m, & else \end{cases} \quad (19)$$

Here, $TD_m^{D/D2}$ defines a newly predicted position for m^{th} stored member in CBOA and the corresponding fitness value is described as $\delta D_m^{D/D2}$.

In third stage, the cooking student enhanced their ability depends on the individual practices. The updating procedure increases the local search and exploitation capability to find the optimum solutions which are adjacent to the predicted locations. As a result, the position is determined as follows:

$$td_{m,n}^{D/D3}=\begin{cases} td_{m,n}+B_n^{\ell,local}+\rho.\left(B_n^{\upsilon,local}-B_n^{\ell,local}\right), & n=\rho \\ td_{m,n}, & n\neq\rho \end{cases} \quad (20)$$

Here, $td_i^{D/D3}$ represents the new status for m^{th} stored candidate of CBOA depends on third strategy and the n^{th} coordinate is indicated as $td_{m,n}^{D/D3}$. Moreover, ρ

implies the randomly selected number of the set $\{1,2,...,q\}$. The enhanced random position depends on the fitness value, which is mathematically expressed as,

$$TD_m = \begin{cases} TD_m^{D/D3}, & TD_m^{D/D3} < \delta_m; \\ TD_m, & else \end{cases} \quad (21)$$

Step 5: Termination

The above said methods are followed and iterated until the best solution is found.

3.4. Feature Extraction

The image Q_s^{DUN} is given to a feature extraction module for extracting the important features to make the further process in an effectual way. Here, the GLCM features, CLBP, DWT, LVP, PHoG, LOOP, LDTP and geometric features are extracted.

3.4.1. GLCM texture features

GLCM features [14] are used to achieve a spatial dependency among the image pixels. Moreover, GLCM is a matrix, in which the order (number of rows and columns) of the matrix is same as the number of grey values of the image. Here, the matrix element $O(M,N|\Delta_\omega,\Delta_\varpi)$ are frequency separated using a pixel distance $(\Delta_\omega,\Delta_\varpi)$. The GLCM extracts the statistical measures from the matrix. However, it is mostly used on grey level image matrices to accomplish significant features such as entropy, contrast, correlation, ASM and energy.

a) Entropy

Entropy is defined as the amount of continuous loss of energy owing to severe heat. Moreover, the entropy is indicated as J_1,

$$J_1 = -\sum_{M=0}^{R-1}\sum_{N=0}^{R-1} O(M,N)\times\log(O(M,N)) \quad (22)$$

Where, R signifies the quantity of gray levels. M,N are the pixel elements of matrix O.

b) Contrast

In the GLCM matrix, the grey level difference is expressed by contrast [20], which is denoted as. J_2.

$$J_2 = \sum_{b=0}^{R-1} b^2 \left\{ \sum_{M=1}^{R}\sum_{N=1}^{R} O(M,N) \right\}, \ |M-N| = b \quad (23)$$

Where, the deviation of M and N pixel is indicated as b.

c) Correlation

It is referred to a measure of grey level dependency and is stated as the ratio of equivalence of the pixel to its neighbor measures. As a result, the correlation expression is given as J_3,

$$J_3 = \sum_{M=0}^{R-1}\sum_{N=0}^{R-1} \frac{\{M\times N\}\times O(M,N) - \{\chi_\omega \times \gamma_\varpi\}}{\sigma_\omega \times \sigma_\varpi} \quad (24)$$

Here, χ_ω and χ_ϖ specifies a mean of O_ω hand O_ϖ. Furthermore, the standard deviation of O_ω and O_ϖ is denoted as σ_ω and σ_ϖ.

d) ASM

ASM represents an even distribution of grey levels that has a general limit of 1, with a measurement 1 referring to the constant image. The ASM feature is specified as J_4

$$J_4 = \sum_{M=0}^{R-1}\sum_{N=0}^{R-1} \{O(M,N)\}^2 \quad (25)$$

e) Energy

The grading of an image is established by the energy features, which also determine its homogeneity. When, the degree of homogeneity is more, the energy level is always high. Furthermore, the energy parameter is represented as J_5

$$J_5 = \sum_{M=0}^{R-1}\sum_{N=0}^{R-1} [O(M,N)]^2 \quad (26)$$

3.4.2. Geometric features

The following are the geometric characteristics [21] acquired during the feature extraction phase:

a) Area

The area of the segmented lung infection zone is calculated by counting the total number of pixels in an image array with the value 1.

$$J_6 = A[1] \quad (27)$$

Here, $A[\ ]$ defines the patterns counting and J_6 specifies the area.

b) Perimeter

Perimeter is used to compute the distance between the individual's adjacent pixel pair for encompassing the edge region. The perimeter characteristic is denoted by the symbol J_7.

c) Irregularity index

The irregularity of affected area (J_8) defines the tuberculosis, which is expressed as

$$J_8 = \frac{4\pi \times J_6}{\left(J_7\right)^2} \tag{28}$$

Where, J_6 indicates the area and J_7 specifies the perimeter.

3.4.3. CLBP

CLBP [15] is an advanced form of Local Binary Pattern (LBP) operator that assigns a 2 dimensional-bit code to the center pixel based on the grey measurements of a local neighborhood. Moreover, CLBP utilized two bits for every unique neighbor for encoding the magnitude and sign of grey value difference among the center and its neighborhood pixels. The CLBP [9] pattern was created to extract the local images for texture categorization. The deviation between the pixel c_μ and neighbor pixel c_ξ is assessed by $Dif_\xi = c_\xi - c_\mu$. It is expressed as,

$$Dif_\xi = \hbar_\xi * \Im_\xi \tag{29}$$

Where,

$$\Im_\xi = \left|Dif_\xi\right| \tag{30}$$

$$\hbar_\xi = \begin{cases} 1 & Dif_\xi \geq 0 \\ -1 & Dif_\xi \leq 0 \end{cases} \tag{31}$$

Where, $\hbar_\xi$ implies the sign factor and $\Im_\xi$ denotes a magnitude factor. Furthermore, the CLBP features are denoted as J_9.

3.4.4. DWT

DWT [16] is the most important technique for feature extraction, and it is used for refining the wavelet coefficients from CXR images. Here, a wavelet finds the frequency level of data in the signal component, which is crucial for recognition. Here, the image is divided into spatial frequency units and it was extracted from the low-low (LL) sub-bands. Still, the high-low (HL) bands provided superior outcome than LL sub-bands.

$$J_{10} = \begin{cases} Yy_{M,N} = \sum S\left(\varepsilon\right)\kappa * S\left(\varepsilon - 2MN\right) \\ Yy_{M,N} = \sum S\left(\varepsilon\right)\varsigma * S\left(\varepsilon - 2MN\right) \end{cases} \tag{32}$$

The term $Yy_{M,N}$ defines the component attribute of signal $S\left(\varepsilon\right)$. Moreover, κ implies the high-pass filter and ς specifies the low-pass filter. Here J_{10} implies the DWT feature.

3.4.5. LVP Feature

LVP [17] is a one-dimensional direction and structural information generator for local textures. It calculates the referenced and the adjacent pixels in different directions and distances. The vector direction $B_{\varphi,\theta}(W_\phi)$ of a referenced pixel W_ϕ using a local sub-region X is denoted by,

$$B_{\varphi,\theta}(W_\phi) = (X(W_{\varphi,\theta}) - X(W_\phi)) \tag{33}$$

Where, the direction of adjacent and referenced pixel is denoted as φ, θ specifies the distance amongst the referenced and adjacent pixels. Moreover, the transform ratio is utilized for generating a weight vector in dynamic linear decision function, which is embedded by a unique 8-bit binary form for each LVP. Moreover J_{11} specifies the LVP feature.

3.4.6. PHOG Feature

The HoG feature of each image sub-region on every resolution level constitutes a PHOG [18] feature. The following details are needed for obtaining the PHOG features.

Step 1: The edge contours of the image are extracted to create the subsequent processing.

Step 2: In various pyramidal levels, the cells are segregated from the images.

Step 3: The HOG of every grid was determined for every pyramid resolution values. Here, the local shape is indicated by an edge orientation histogram. From step 1, the edge contours of original images were located, and then the orientation gradient was estimated.

Step 4: To construct the PHOG descriptive for an image, all the HOG vectors in every pyramid resolution were combined. Here, the spatial information of an image is comprised by incorporating every HOG vectors. Each HOG is resolved and combined to unity. Moreover, the outcome of PHOG features is specified as J_{12}.

3.4.7. LOOP Feature

The design of nonlinear combination of LDP and LBP forms the LOOP [19]. The LOOP function ignores the constraints of LDP and LBP. Furthermore, kirsch mask is used for the encoding process of LDP. The incorporation of such design is allocated by the binarization weights of corresponding neighboring pixel, then it goes to the Kirsch output's strength on the direction of pixels c_μ and g_μ .Here, the LOOP feature of pixel $\left(c_\mu, g_\mu\right)$ is given by,

$$LOOP\left(c_{\mu}, g_{\mu}\right)=\sum_{l=0}^{7} \wp\left(\zeta_{l}-\zeta_{\mu}\right).2^{\aleph_{l}} \tag{34}$$

Where, $\wp(c)=\begin{cases}1 & if\ c \geq 0 \\ 0 & otherwise\end{cases}$, ζ_l represents the intensity of neighborhood pixel and ζ_{μ} specifies the intensity of central pixel, $\aleph_l$ lies in between of(0-7), and the output image is specified as J_{13}.

3.4.8. LDTP Feature

LDTP [20] is a framework that allows the compact encoding for both contrast information and directional pattern elements using local derivative variations. The LDTP was represented as an eight-bit pattern code that was allocated to each pixel on the image. In contrast to Local Directional Number (LDN) and LDTP, the LDTP utilized different compass masks. Moreover, the contrast data was encoded by contrasting the outlying and center pixels. Moreover, the Local Ternary Pattern (LTP) concept is applied to generate the final LDTP code. Since the edge response has minimum sensitive for illumination and noise level, then the outcome of LDTP feature indicates the local primitives in consistent way for extracting lot of information. Furthermore, the LDTP model is designed using an indicator $\Re$, which is given by,

$$\Re\left(\hat{\lambda}, \Xi\right)=\begin{cases}+1 & if\ \hat{\lambda} \geq 0 \quad and\ \Xi \geq 0 \\ -1 & if\ \hat{\lambda} \leq 0 \quad and\ \Xi \leq 0 \\ 0 & otherwise\end{cases} \tag{35}$$

Here, $\hat{\lambda}$, Ξ are the numerical values and the outcome of LDTP is represented as J_{14}

Hence, the entire outcome of feature extraction process is specified as

$$J=\left\{J_1, J_2, J_3, J_4, J_5, J_6, J_7, J_8, J_9, J_{10}, J_{11}, J_{12}, J_{13}, J_{14}\right\} \tag{36}$$

3.5. TB detection using DbneAlexNet

The feature vector J is passed to the DbneAlexNet [22] to detect TB effectively and the weights of this network are effectively trained using CLBO, which is a consolidation of CBOA and HLBO. The structure of DbneAlexNet is discussed elaborately in the below part.

3.5.1. Architecture of DbneAlexNet

The DbneAlexNet contains the convolutional which is followed by the batch normalization layer, Max pooling, flatten, dense layer and dropout layers. Figure 3 deliberates the architecture of DbneAlexNet. The feature vector J is applied as the input of DbneAlexNet. Here, the Exponential linear unit (Elu) activation layer is used as the substitution of rectified linear unit (ReLU) activation layer. Moreover, batch normalization is utilized to solve the internal covariate shift issues occurred on neural networks owing to the fluctuations of input data distribution. It is caused by the changing number of variables in the previous one. Dropout is another mechanism used in the model. During training, the dropout method is employed to neglect the randomly picked neurons. Moreover, the outcome image of DbneAlexNet is indicated as Q_f^{Dbne}.

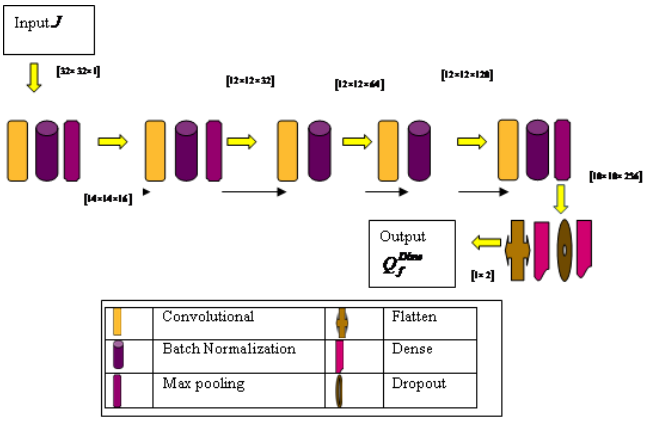

Fig. 3. Architecture of DbneAlexNet

3.5.2. Training of DbneAlexNet using TCLBO

The TCLBO algorithm tunes the DbneAlexNet parameters during the TB detection phase. Here, the TSA [25] presents a set of principles which employs the tangent function to find the best solution. Furthermore, the tangent function facilitates the balance between the exploitation and exploration search. It is also used to neglect the local minima. Furthermore, this algorithm is employed to enhance convergence capacity.

Fitness Function

Fitness function is considered as the major criteria for achieving the optimal solution of TCLBO. It is the deviation of targeted outcome and the outcome of DbneAlexNet.

$$Fitness=\frac{1}{v}\sum_{f=1}^{v}\left[Q_f^{*}-Q_f^{Dbne}\right]^2 \tag{37}$$

Where, v indicated the entire counting of CXR images, Q_f^{*} implies the targeted output and Q_f^{Dbne} represents the outcome of DbneAlexNet.

Updated Equation of TCLBO

For attaining the solution of TCLBO, the TSA [25] is merged to CLBO. The updated equation of TCLBO is given as,

$$t_{m,n}(r+1)=\frac{1}{2\rho.o}\left[\rho.L_{m,n}^{H}(1-\rho.o)+\rho.I_{u_{m,n}}(1+\rho.o)\right] \quad (38)$$

The TSA is included to increase convergence capacity. The updated equation of TCLBO is then obtained by the following expressions,

$$t_{m,n}(r+1)=t_{m,n}(r)+step*\tan(\theta)*\left(t_{m,n}(r)-Opt\,K_m(r)\right) \quad (39)$$

$$t_{m,n}(r+1)=t_{m,n}(r)\left[1+step*\tan(\theta)\right]-step*\tan(\theta)Opt\,K_m(r) \quad (40)$$

$$t_{m,n}(r)=\frac{t_{m,n}(r+1)+step*\tan(\theta)Opt\,K_m(r)}{1+step*\tan(\theta)} \quad (41)$$

Subtract $t_{m,n}(r)$ from the update equation of CLBO,

$$t_{m,n}(r+1)-t_{m,n}(r)=\frac{1}{2\rho.o}\left[\rho.L_{m,n}^{H}(1-\rho.o)+\rho.I_{u_{m,n}}(1+\rho.o)\right]-t_{m,n}(r) \quad (42)$$

Substitute equation (41) in L.H.S of equation (42)

$$t_{m,n}(r+1)-t_{m,n}(r)=\frac{1}{2\rho.o}\left[\rho.L_{m,n}^{H}(1-\rho.o)+\rho.I_{u_{m,n}}(1+\rho.o)\right]-\frac{t_{m,n}(r+1)+step*\tan(\theta)Opt\,K_m(r)}{1+step*\tan(\theta)} \quad (43)$$

$$t_{m,n}(r+1)-\frac{t_{m,n}(r+1)}{1+step*\tan(\theta)}=\frac{1}{2\rho.o}\left[\rho.L_{m,n}^{H}(1-\rho.o)+\rho.I_{u_{m,n}}(1+\rho.o)\right]-\frac{+step*\tan(\theta)Opt\,K_m(r)}{1+step*\tan(\theta)}+t_{m,n}(r) \quad (44)$$

$$\frac{t_{m,n}(r+1)(1+step*\tan(\theta))-t_{m,n}(r+1)}{1+step*\tan(\theta)}=\frac{\left[\begin{array}{l}(1+step*\tan(\theta))\left[\rho.L_{m,n}^{H}(1-\rho.o)+\rho.I_{u_{m,n}}(1+\rho.o)\right]\\-(step*\tan(\theta)Opt\,K_m(r))(2\rho.o)\\+(2\rho.o)(1+step*\tan(\theta))t_{m,n}(r)\end{array}\right]}{(2\rho.o)(1+step*\tan(\theta))} \quad (45)$$

$$t_{m,n}(r+1)\left[1+step*\tan(\theta)-1\right]=\frac{\left[\begin{array}{l}(1+step*\tan(\theta))\left[\rho.L_{m,n}^{H}(1-\rho.o)+\rho.I_{u_{m,n}}(1+\rho.o)\right]\\-(step*\tan(\theta)Opt\,K_m(r))(2\rho.o)\\+(2\rho.o)(1+step*\tan(\theta))t_{m,n}(r)\end{array}\right]}{(2\rho.o)} \quad (46)$$

$$t_{m,n}(r+1)\left[step*\tan(\theta)\right]=\frac{\left[\begin{array}{l}(1+step*\tan(\theta))\left[\rho.L_{m,n}^{H}(1-\rho.o)+\rho.I_{u_{m,n}}(1+\rho.o)\right]\\-(step*\tan(\theta)Opt\,K_m(r))(2\rho.o)\\+(2\rho.o)(1+step*\tan(\theta))t_{m,n}(r)\end{array}\right]}{(2\rho.o)} \quad (47)$$

$$t_{m,n}(r+1)=\frac{1}{(2\rho.o)(step*\tan(\theta))}\left[\begin{array}{l}(1+step*\tan(\theta))\left[\rho.L_{m,n}^{H}(1-\rho.o)+\rho.I_{u_{m,n}}(1+\rho.o)\right]\\-(step*\tan(\theta)Opt\,K_m(r))(2\rho.o)\\+(2\rho.o)(1+step*\tan(\theta))t_{m,n}(r)\end{array}\right] \quad (48)$$

Table 1: Pseudo code for TCLBO

SL. No	Pseudo code of designed TCLBO
1	Input: $t_{m,n}(r),\delta,o,\rho$
2	Output: $td_{m,n}(r+1)$
3	Start
4	Set population size G and iterations r
5	Generate the initial population matrix t
6	Evaluate the fitness by equation (8)
7	For $r=1$
8	Sorting the matrix TD by equation (9)
9	Update a set of chef instructors I and the best member C_{best}
10	Go step 3
11	For $m=1$ to G_h
12	Find $TD_m^{h/D1}$ by equation (10)
13	Update TD_m by equation (11)
14	Compute the upper and lower bound variables by Equation. (13) and (14)
15	Find $TD_m^{h/D2}$ using Equation (12)
16	End
17	End phase 1
18	**Begin step 4**
19	For $m=G_{h+1}$ to G
20	Find a chef instructor
21	Compute $t_{m,n}(r+1)$ using equation (48)
22	Update TD_m using equation(17)
23	Compute $td_m^{D1/D2}$ using equation (18)
24	Update TD_m using equation (19)
25	Compute $td_m^{D1/D5}$ using equation (20)
26	Update TD_m using equation. (21)
27	End
28	End phase 2
29	Return back to the best solution
30	End
31	End

Hence, the updated solution of TCLBO is obtained from equation (48), in which $t_{m,n}(r+1)$ indicates the updates solution, $step$ represents the move size. The Pseudo code for TCLBO is described in table 1.

4. RESULTS AND DISCUSSION

The outcome of designed TCLBO_DbneAlexNet is computed in this section. Here, the comparative evaluation is attained by assessing the performance of TCLBO_DbneAlexNet as that of the existing methods.

4.1. Experimental outcomes

Figure 4(i) deliberates the image outcome of devised TCLBO_DbneAlexNet for TB detection. Here, the input image is deliberated in figure 4 a). The pre-processed, segmented, CLBP, DWT, LVP, LOOP and LDTP images are displayed in figure 4 b), 4 c), 4 d), 4 e), 4 f), 4 g) and 4 h) respectively. Figure 4(ii) illustrates the Experimental outcomes of a) Input CXR image and heat map of

Tuberculosis with Lung mass class b) Input CXR image and heat map of Tuberculosis with infiltration class

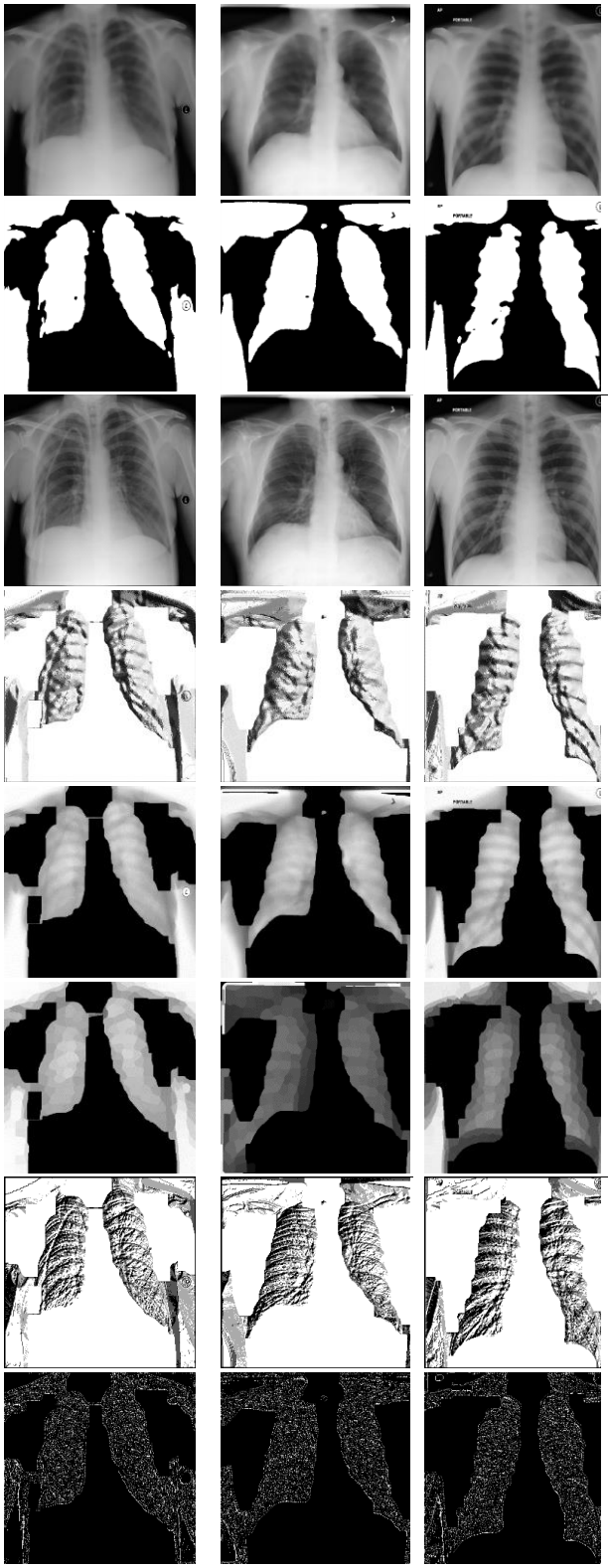

Fig. 4. (i). Experimental outcomes, a) input image, b) pre-processed image, c) segmented image, d) CLBP, e) DWT, f) LVP, g) LOOP, h)LDTP,

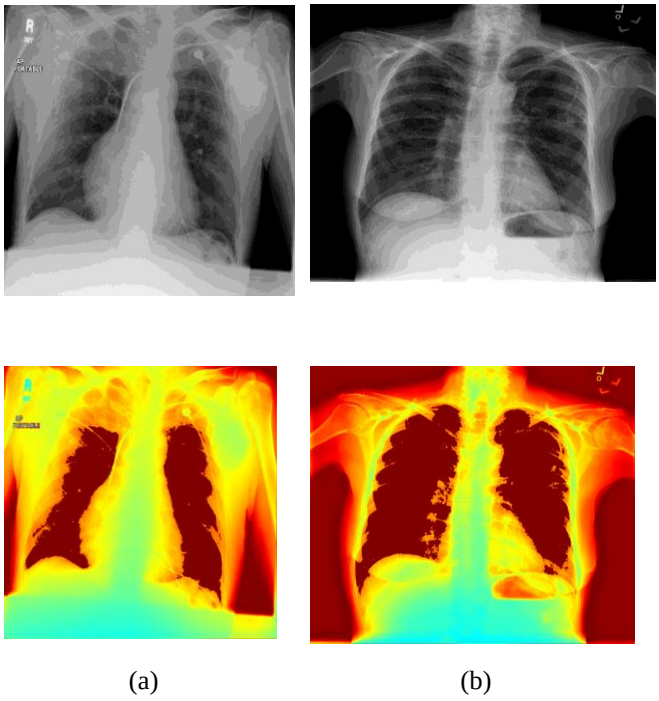

(a) (b)

Fig. 4. (ii). Experimental outcomes a) Input CXR image and heat map of Tuberculosis with Lung mass class b) Input CXR image and heat map of Tuberculosis with infiltration class.

4.2. Dataset description

The Chest X-ray Database [6] is employed to provide the normal images as well as the chest X-ray images with positive TB disorder. This dataset contains 3500 images, in which 700 TB images are widely available.

4.3. Evaluation metrics

Accuracy, PPV, NPV, TPR and TNR are the metrics considered for estimation of TCLBO_DbneAlexNet in TB detection.

4.3.1. Accuracy

Accuracy is represented as a standard metric that truly identify the presence of disease amongst the entire counting of samples.

$$Accuracy = \frac{T_{pos} + T_{neg}}{T_{pos} + T_{neg} + N_{pos} + N_{neg}} \tag{49}$$

Where, T_{pos} specifies the true positive and N_{pos} denotes the false positives. Similarly, N_{neg} and T_{neg} are the representation of false negative and true negative.

4.3.2. PPV

PPV is stated as the proportion of patients exactly detected as positive to those who got a positive test result.

$$PPV = \frac{T_{pos}}{T_{pos} + N_{pos}} \tag{50}$$

4.3.3. NPV

NPV is defined as the proportion of patients exactly detected as negative to those who got a negative test result.

$$NPV = \frac{T_{neg}}{T_{neg} + N_{neg}} \tag{51}$$

4.3.4. TPR

The entire counts of positive result detected by the patients is denotes as TPR. It is also termed as sensitivity.

$$TPR = \frac{T_{pos}}{T_{pos} + N_{neg}} \tag{52}$$

4.3.5. TNR

The entire counts of negative result detected by the patients are defined as TNR. It is also called as specificity.

$$TNR = \frac{T_{neg}}{T_{neg} + N_{pos}} \tag{53}$$

4.4. Comparative methods

The conventional methods utilized for the comparison of proposed TCLBO_DbneAlexNetare E-B net [13], CCNSE [12], VGG-UNet [1] Ensemble learning [4] and CLBO_DenseNet.

4.5. Comparative evaluation

In this section, the comparative valuation of TCLBO_DbneAlexNetis discussed with respect to the evaluation parameters by altering the training set and the K-value. Here, E-TBNet, CCNSE, VGG-UNet, Ensemble learning and CLBO_DenseNet the existing approaches included for the comparative assessment of TCLBO_DbneAlexNet.

4.5.1. Evaluation with training set

The evaluation of TCLBO_DbneAlexNet in TB detection is performed using different training set is deliberated in figure 5. The evaluation with respect to accuracy is shown in figure 5 a).For the training set=70%, the accuracy of TCLBO_DbneAlexNet is 0.958, whereas the other techniques like E-B Net, CCNSE, VGG-UNet, Ensemble learning and CLBO_DenseNet attained the accuracy of 0.825, 0.846, 0.875, 0.906 and 0.935 respectively. Hence, the TCLBO_DbneAlexNet has 13.85%, 11.63%, 8.640%, 5.393% and 2.354% of enhanced performance than others. In figure 5b), the comparative valuation with regards to PPV metrics is displayed. While considering 80% of training set, the PPV values like 0.807, 0.817, 0.857, 0.896, 0.916 and 0.936 are attained by the E-TBNet, CCNSE, VGG-UNet, Ensemble learning, CLBO_DenseNet and the proposed TCLBO_DbneAlexNet. Here, the TCLBO_DbneAlexNet has 13.71%, 12.63%, 8.398%, 4.219% and 2.083% of superior performance than others. Besides, the evaluation in connection with NPV is shown in figure 5 c). Here, the E-TBNet, CCNSE, VGG-UNet, Ensemble learning, CLBO_DenseNet and the proposed TCLBO_DbneAlexNet attained the NPV values of 0.745, 0.766, 0.797, 0.826, 0.855 and 0.873 respectively using 60% of training set. From this estimation, the proposed TCLBO_DbneAlexNet attained 14.59%, 12.19%, 8.630%, 5.323% and 2.013% of better performance than other approaches. Likewise figure 5 d) revealed the comparative evaluation with regards to TPR. Here, the proposed TCLBO_DbneAlexNet attained the TPR of 0.916 in 70% of training set. For the similar training set the TPR of E-TBNet is 0.785, CCNSE is 0.806, VGG-UNet is 0.835, Ensemble learning is 0.866 and CLBO_DenseNet is 0.895. Hence the TCLBO_DbneAlexNet achieved 14.31%, 11.99%, 8.867%, 5.473% and 2.297% of performance enhancement while compared to others. Furthermore, the comparative valuation in connection with TNR is shown in figure 5 e). The TNR value of TCLBO_DbneAlexNet is 0.928 using 80%training set. Here, the E-TBNet, CCNSE, VGG-UNet, Ensemble learning, and CLBO_DenseNethas the TNR of 0.797, 0.807, 0.847, 0.886 and 0.906 while considering the same training set. Hence, the TCLBO_DbneAlexNet attained the performance enhancement of 14.08%, 12.99%, 8.721%, 4.508% and 2.354% than other methods.

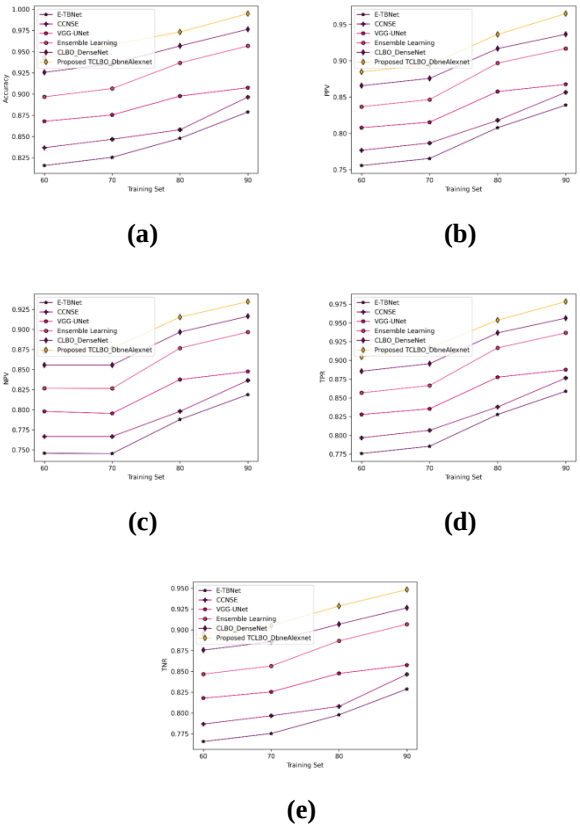

Fig.5. Evaluationin terms of training set, a) Accuracy, b) PPV, c) NPV, d) TPR, e) TNR

4.5.2. Assessment with K-value

The analysis of TCLBO_DbneAlexNet for TB detection using different K-value is displayed in figure 6. Here, figure 6 a) deliberates the evaluation of TCLBO_DbneAlexNet regards to accuracy is shown in figure 6 a). For the K-value=7, the accuracy of TCLBO_DbneAlexNet is 0.967, while the other techniques such asE-TBNet, CCNSE, VGG-UNet, Ensemble learning and CLBO_DenseNet reached the accuracy of 0.835, 0.856, 0.885, 0.916 and 0.945. Here, the TCLBO_DbneAlexNet attained13.61%, 11.40%, 8.446%, 5.228% and 2.217% of performance enhancement compared to others. The comparative estimation in terms of PPV is illustrated in figure 6 b). For considering the K-value of 8, the PPV values of E-TBNet, CCNSE, VGG-UNet, Ensemble learning, CLBO_DenseNet and the proposed TCLBO_DbneAlexNetare are 0.817, 0.827, 0.867, 0.906, 0.926 and 0.948 respectively. Hence, the TCLBO_DbneAlexNet attained 13.78%, 12.71%, 8.535%, 4.411% and 2.302% performance enhancement than others. Likewise, the estimation in connection with NPV is illustrated in figure 6 c). Here, the NPV of proposed TCLBO_DbneAlexNet is 0.892. The NPV of E-TBNet is 0.762, CCNSE is 0.783, VGG-UNet is 0.814, Ensemble learning is 0.843 and CLBO_DenseNetis 0.872 using the K-value of 6. Hence, the proposed TCLBO_DbneAlexNet has 14.55%, 12.20%, 8.715%, 5.480% and 2.241% of improved performance with respect to other approaches. Similarly, figure 6 d) shown the comparative analysis regarding TPR. The proposed TCLBO_DbneAlexNet has the TPR of 0.935 using the K-value=7. For the similar K-value the TPR of E-TBNet, CCNSE, VGG-UNet, Ensemble learning and CLBO_DenseNet are 0.805, 0.826, 0.855, 0.886 and 0.915. Therefore, the TCLBO_DbneAlexNet got 13.91%, 11.63%, 8.570%, 5.245% and 2.132% of enhanced performance in connection with others. Moreover, estimation in connection with TNR is revealed in figure 6 e). Here, the TNR value of TCLBO_DbneAlexNet is 0.947 by the K-value of 8. Here, the TNR of E-TBNet is 0.817, CCNSE is 0.827, VGG-UNet is 0.867, Ensemble learning is 0.906, and CLBO_DenseNet is 0.926.

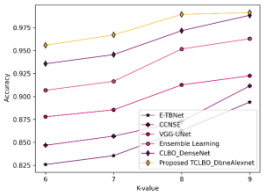

(a)

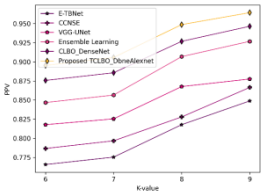

(b)

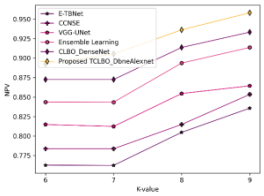

(c)

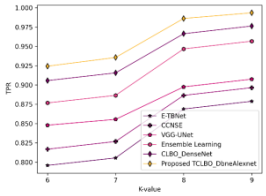

(d)

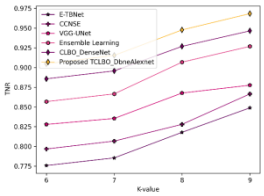

(e)

Fig 6. Evaluation with K-value, a) accuracy, b) PPV, c) NPV, d) TPR, e) TNR

4.5. Analysis using training accuracy versus testing accuracy

The validation of TCLBO_DbneAlexNet in terms of training accuracy and testing accuracy against change of iteration is delineated in figure 9. It is proven that the training and testing accuracy increases as the total number of iterations increases. From the analysis, it is observed that the TCLBO_DbneAlexNet attained a training accuracy of 0.958 and a testing accuracy of 0.948 for 300 iterations.

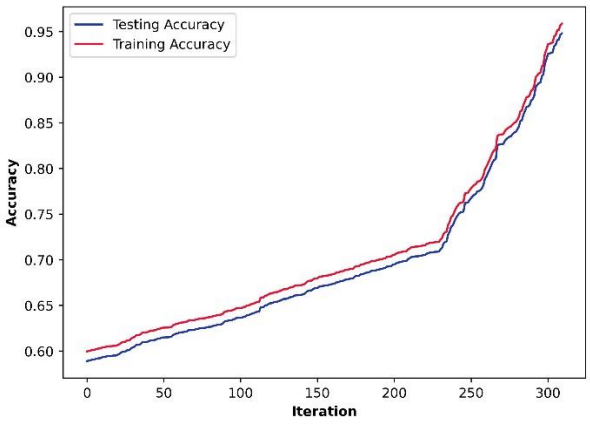

Fig.7. Validation of TCLBO_DbneAlexNet using training accuracy vs testing accuracy

4.6 Algorithmic methods

The TCLBO_DbneAlexNet for TB detection is evaluated and its performance is compared with respect to other algorithms like Rider Optimization Algorithm (ROA) [26] +DbneAlexnet, TSA[25]+DbneAlexnet, HLBO[24]+ DbneAlexnet and CLBO+DbneAlexnet.

4.6.1. Algorithmic evaluation

The estimation with regards to different algorithms are displayed in figure 7. Here the algorithms like ROA+DbneAlexnet, TSA+DbneAlexnet, HLBO+DbneAlexnet, CLBO+DbneAlexnet and the Proposed TCLBO+DbneAlexnet are considered for the assessment. Here, figure 7 a) represents the assessment in terms of accuracy. Here, the accuracy of proposed TCLBO+DbneAlexnet is 0.967 with respect to the solution size of 30. The other method likeROA+DbneAlexnet, TSA+DbneAlexnet, HLBO+DbneAlexnet and CLBO+DbneAlexnet has the accuracy of 0.917, 0.924, 0.934 and 0.947. The assessment in terms of PPV is deliberated in figure 7 b). Here, the PPV like 0.826, 0.831, 0.846, 0.852 and 0.874 are attained by the ROA+DbneAlexnet, TSA+DbneAlexnet, HLBO+DbneAlexnet, CLBO+DbneAlexnet and the proposed TCLBO+DbneAlexnet in the solution size of 10. Moreover, the evaluation regards to NPV is shown in figure 7 c). For the solution size=20, the ROA+DbneAlexnet, TSA+DbneAlexnet, HLBO+DbneAlexnet, CLBO+DbneAlexnet and the Proposed TCLBO+DbneAlexnet attained the NPV of 0.836, 0.825, 0.846, 0.852 and 0.873 respectively. Likewise, the assessment with regards to TPR is shown in figure 7 d). Considering the solution size 0f 40, the TPR of proposed TCLBO+DbneAlexnet is 0.964, whereas the ROA+DbneAlexnet, TSA+DbneAlexnet, HLBO+DbneAlexnet and CLBO+DbneAlexnet attained the TPR of 0.917, 0.927, 0.934 and 0.942. Moreover, the analysis in connection with TNR is shown in figure 7 e). Here, the TNR values like 0.872, 0.884, 0.892, 0.905 and 0.928 are attained by the ROA+DbneAlexnet, TSA+DbneAlexnet, HLBO+DbneAlexnet, CLBO+DbneAlexnet and the proposed TCLBO+DbneAlexnet while considering the solution size of 30.

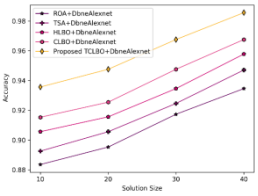

(a)

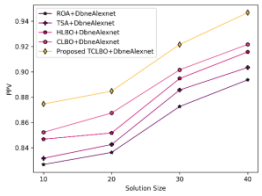

(b)

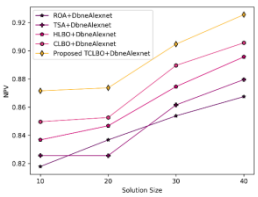

(c)

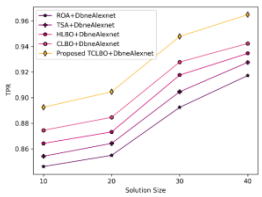

(d)

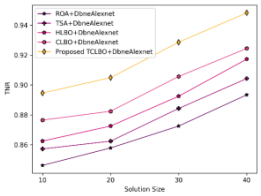

(e)

Fig.8. Algorithmic analysis a) Accuracy, b) PPV, c) NPV, d) TPR, e) TNR

4.7. Comparative discussion

The comparative discussion of proposed TCLBO_DbneAlexNet is displayed in table 2. Here, the performance of TCLBO_DbneAlexNet is validated by comparing it with other existing approaches. Moreover, the experimental outcome of TCLBO_DbneAlexNet and other existing techniques in terms of different training data K-values are displayed. In training data variation, the accuracy, PPV, NPV, TPR and TNR of proposed TCLBO_DbneAlexNet are 0.994, 0.964,0.934, 0.978 and 0.948 respectively. From this, it is clearly noted that, the superior value of accuracy, PPV, NPV, TPR and TNR values are attained in K-value based assessment. For K value=9, the maximum accuracy of proposed TCLBO_DbneAlexNet is 0.991, whereas the other methods like E-TBNet, CCNSE, VGG-UNet, Ensemble learning and CLBO_DenseNet attained the accuracy of 0.893, 0.911, 0.922, 0.962 and 0.988 respectively. Similarly, the superior PPV value of 0.964 is achieved by the proposed TCLBO_DbneAlexNet, in which the PPV of other existing approaches are 0.848, 0.866, 0.877, 0.926, and 0.946. Moreover, the NPV of proposed TCLBO_DbneAlexNet is 0.958, whereas the E-TBNet, CCNSE, VGG-UNet, Ensemble learning and CLBO_DenseNet has the NPV OF0.835, 0.853, 0.864 0.913 and 0.933. Likewise, the maximum TPR value of proposedTCLBO_DbneAlexNet is 0.993. Here the TPR of 0.878, 0.896, 0.907, 0.956 and 0.976 and are observed by the E-TBNet, CCNSE, VGG-UNet, Ensemble learning and CLBO_DenseNet. Similarly, the proposed TCLBO_DbneAlexNet attained the better TNR value of 0.968, while the TNR of E-TBNet is 0.848, CCNSE is 0.866 VGG-UNet is 0.877 Ensemble learning is 0.926 and CLBO_DenseNet is 0.946.

Table 2. Comparative discussion

	Metrics	E-TBNet	CCNSE	VGG-UNet	Ensemble learning	CLBO_DenseNet	Propoded TCLB0_Dbne AlexNet
Training set=90%	*Accuracy*	0.878	0.896	0.907	0.956	0.976	0.994
	PPV	0.838	0.856	0.867	0.916	0.936	0.964
	NPV	0.818	0.836	0.847	0.896	0.916	0.934
	TPR	0.858	0.876	0.887	0.936	0.956	0.978
	TNR	0.828	0.846	0.857	0.906	0.926	0.948
K-value=9	*Accuracy*	0.893	0.911	0.922	0.962	0.988	**0.991**
	PPV	0.848	0.866	0.877	0.926	0.946	**0.964**
	NPV	0.835	0.853	0.864	0.913	0.933	**0.958**
	TPR	0.878	0.896	0.907	0.956	0.976	**0.993**
	TNR	0.848	0.866	0.877	0.926	0.946	**0.968**

5. Conclusion

According to WHO reports, TB is considered as a leading disease, with a significant fatality rate. Several technologies have been devised for the TB disease detection on its earlier stage; however, some of these techniques required good medical experts, that may be a significant challenge. This work establishing an automatic system to identify TB disorder using the proposed optimization algorithm called TCLBO_DbneAlexNet. Pre-processing is the initial step, in which the input image is subjected to filtering process. It is accomplished by an adaptive bilateral filter, which removes the noise. Following that, segmentation is performed with the help of Double U-Net model, which is trained using the CLBO. Besides, the GLCM features, CLBP, DWT, LVP, and geometrical features are extracted in feature extraction phase. By merging all of these features to form the feature vector. The feature vector is given to the TB detection stage, where the detection is carried out using DbneAlexNet, which is trained by the proposed TCLBO.

Moreover, predictive analysis is performed to classify the TB class, heat maps for localization, and identification of the lung abnormalities. Moreover, the TCLBO_DbneAlexNet provided better accuracy of 0.991, PPV of 0.964, NPV of 0.958TPR of 0.993, and TPR of 0.968.In future work, the integration of several hybrid optimization algorithms and different feature extraction techniques will be considered for getting even more precise result.

References

[1] O. Yadav, K. Passi, and C.K. Jain, "Using deep learning to classify X-ray images of potential tuberculosis patients" In proceedings of 2018 IEEE International Conference on Bioinformatics and Biomedicine (BIBM), pp. 2368-2375, 2018.

[2] W.Y.N. Naing, and W.Y.N. Htike, x "Advances in automatic tuberculosis detection in chest x-ray images", Signal & Image Processing, vol.5, no.6, pp.41, 2014.

[3] L. An, K. Peng, X.Yang, P.Huang, P. Luo, P. x Feng, and B. Wei, "E-TBNet: Light Deep Neural Network for Automatic Detection of Tuberculosis with X-ray DR Imaging", Sensors, vol. 22, no.3, pp.821. 2022.

[4] M. Ayaz, F.Shaukat, and G. Raja, "Ensemble learning based automatic detection of Tuberculosis using hybrid feature descriptors", Physical and Engineering Sciences in Medicine, vol. 44, no.1, pp.183-194. 2021.

[5] S.Urooj, S. Suchitra, L. xKrishnasamy, N. Sharma, and N. Pathak, "Stochastic Learning-Based Artificial Neural Network Model for an Automatic Tuberculosis Detection System Using Chest X-Ray Images", IEEE Access, vol.10, pp.103632-103643, 2022.

[6] TB Chest X-ray Database available at "https://www.kaggle.com/datasets/tawsifurrahman/tuberculosis-tb-chest-xray-dataset",accessed on 2023.

[7] N.Xue, D. x You, S.Candemir, S.Jaeger, S.Antani, L.R. Long, and G.R.Thoma, "Chest x-ray image view classification", In proceedings of 2015 IEEE 28th International Symposium on Computer-Based Medical Systems, pp. 66-71, 2015.

[8] G.R.Panicker, K.S. x Kalmady, J. Rajan, and M.K.Sabu, "Automatic detection of tuberculosis bacilli from microscopic sputum smear images using deep learning methods", Biocybernetics and Biomedical Engineering, vol.38, no.3, pp.691-699, 2018.

[9] T.K.K.Ho, J. Gwak, O. Prakash, J.I. Song, and C.M. Park, "Utilizing pretrained deep learning models for automated pulmonary tuberculosis detection using chest radiography", In proceedings of Intelligent Information and Database Systems: 11th Asian Conference, pp. 395-403, Springer International Publishing, 2019.

[10] E.Tasci, C. Uluturk, and A. Ugur, "A voting-based ensemble deep learning method focusing on image augmentation and preprocessing variations for tuberculosis detection", Neural Computing and Applications, vol.33, no.22, pp.15541-15555, 2021.

[11] A.Singh, G.V.x Pujar, S.A. Kumar, M. Bhagyalalitha, H.S.Akshatha, H.S., Abuhaija, H.S.A.R.x Alsoud, L. Abualigah, N.M. Beeraka, and A.H. Gandomi, "Evolution of machine learning in tuberculosis diagnosis: a review of deep learning-based medical applications", Electronics, vol.11, no.17, pp.2634, 2022.

[12] F.Wu, W.Yang, L.Xiao and J. Zhu, "Adaptive wiener filter and natural noise to eliminate adversarial perturbation", Electronics, vol. 9. no.10, pp.1634, 2020.

[13] [13]D.Jha, M.A. Riegler, D.Johansen, P. Halvorsen, and H.D. Johansen, "Doubleu-net: A deep convolutional neural network for medical image segmentation", In Proceeding of 2020 IEEE 33rd International symposium on computer-based medical systems (CBMS), pp. 558-564, 2020.

[14] N. Zulpe, and V.Pawar, "GLCM textural features for brain tumor classification", International Journal of Computer Science Issues (IJCSI), vol.9, no.3, p.354, 2012.

[15] M. Guermoui, and M.L. Mekhalfi, “A Sparse Representation of Complete Local Binary Pattern Histogram for Human Face Recognition”, arXiv preprint arXiv:1605.09584, 2016.

[16] N. Varuna Shree, and T.N.R. Kumar, "Identification and classification of brain tumor MRI images with feature extraction using DWT and probabilistic neural network", Brain informatics, vol.5, no.1, pp.23-30, 2018.

[17] K.C. Fan, and T.Y. Hung, “A novel local pattern descriptor—local vector pattern in high-order derivative space for face recognition”, IEEE transactions on image processing, vol. 23, no.7, pp.2877-2891, 2014.

[18] Y.,Bai, L. Guo, L. Jin, x and Q.Huang, “A novel feature extraction method using pyramid histogram of orientation gradients for smile recognition”, In Proceedings of 2009 16th IEEE International Conference on Image Processing (ICIP), pp. 3305-3308, 2009.

[19] Q. Chakraborti, B.x McCane, S. Mills, and U. Pal, “LOOP descriptor: Encoding repeated local patterns for fine-grained visual identification of lepidoptera”, arXiv preprint arXiv:1710.09317, pp.1-5, 2017.

[20] A. Chahi, Y. Ruichek, and R.Touahni, “Local directional ternary pattern: A new texture descriptor for texture classification”, Computer vision and image understanding, vol.169, pp.14-27, 2018.

[21] N.S. Lingayat, and M.R. Tarambale, “A computer-based feature extraction of lung nodule in chest x-ray image”, International Journal of Bioscience, Biochemistry and Bioinformatics, vol.3 no.6, p.624.

[22] H. Alaeddine, and M. Jihene, “Deep Batch-normalized eLUAlexNet for Plant Diseases Classification”, In Proceeding of 2021 18th International Multi-Conference on Systems, Signals & Devices (SSD), pp. 17-22, 2021.

[23] E. Trojovská, and M. Dehghani, “A new human-based metaheuristic optimization method based on mimicking cooking training”, Scientific Reports, vol. 12 no.1, pp.14861, 2022.

[24] Trojovsky, P. and Dehghani, M., “Hybrid Leader Based Optimization: A New Stochastic Optimization Algorithm for Solving Optimization Applications”, 2022.

[25] A.Layeb, “Tangent search algorithm for solving optimization problems. Neural Computing and Applications”, vol. 34 no.11, pp.8853-8884, 2022.

[26] D. Binu, and B.S. Kariyappa, “RideNN: A new rider optimization algorithm-based neural network for fault diagnosis in analog circuits”, IEEE Transactions on Instrumentation and Measurement, vol.68, no.1, pp.2-26. 2018

[27] S. Kadry, G. Srivastava, V.Rajinikanth, S. Rho, and Y. Kim, “Tuberculosis Detection in Chest Radiographs Using Spotted Hyena Algorithm Optimized Deep and Handcrafted Features”, Computational Intelligence and Neuroscience, 2022.

[28] [28] V.Ravi, V. Acharya, and V. Alazab, x “A multichannel EfficientNet deep learning-based stacking ensemble approach for lung disease detection using chest X-ray images”, Cluster Computing, vol.26, no.2, pp.1181-1203, 2023.

[29] M., Rahman, Y.Cao, X. Sun, B. Li, and Y. Hao, “Deep pre-trained networks as a feature extractor with XGBoost to detect tuberculosis from chest X-ray”, Computers & Electrical Engineering, vol.93, pp.107252, 2021.

[30] S.M. Fati, E.M. Senan, and N.ElHakim, “Deep and Hybrid Learning Technique for Early Detection of Tuberculosis Based on X-ray Images Using Feature Fusion”, Applied Sciences, vol.12, no.14, pp.7092, 2022.

[31] T. Khatibi, A. Shahsavari, and A. Farahani, “Proposing a novel multi-instance learning model for tuberculosis recognition from chest X-ray images based on CNNs, complex networks and stacked ensemble”, Physical and Engineering Sciences in Medicine, vol. 44, no.1, pp.291-311. 2021.